

# Photoacoustic tomography of joints aided by an Etanercept-conjugated gold nanoparticle contrast agent—an *ex vivo* preliminary rat study

David L Chamberland<sup>1</sup>, Ashish Agarwal<sup>2</sup>, Nicholas Kotov<sup>2</sup>,  
J Brian Fowlkes<sup>3</sup>, Paul L Carson<sup>3</sup> and Xueding Wang<sup>3,4</sup>

<sup>1</sup> Rheumatology Associates, Medford, OR 97504, USA

<sup>2</sup> Department of Chemical Engineering, University of Michigan, Ann Arbor, MI 48109, USA

<sup>3</sup> Department of Radiology, University of Michigan School of Medicine, Ann Arbor, MI 48109-0553, USA

E-mail: [xdwang@umich.edu](mailto:xdwang@umich.edu)

Received 10 October 2007, in final form 3 January 2008

Published 11 February 2008

Online at [stacks.iop.org/Nano/19/095101](http://stacks.iop.org/Nano/19/095101)

## Abstract

Monitoring of anti-rheumatic drug delivery in experimental models and in human diseases would undoubtedly be very helpful for both basic research and clinical management of inflammatory diseases. In this study, we have investigated the potential of an emerging hybrid imaging technology—photoacoustic tomography—in noninvasive monitoring of anti-TNF drug delivery. After the contrast agent composed of gold nanorods conjugated with Etanercept molecules was produced, ELISA experiments were performed to prove the conjugation and to show that the conjugated anti-TNF- $\alpha$  drug was biologically active. PAT of *ex vivo* rat tail joints with the joint connective tissue enhanced by intra-articularly injected contrast agent was conducted to examine the performance of PAT in visualizing the distribution of the gold-nanorod-conjugated drug in articular tissues. By using the described system, gold nanorods with a concentration down to 1 pM in phantoms or 10 pM in biological tissues can be imaged with good signal-to-noise ratio and high spatial resolution. This study demonstrates the feasibility of conjugating TNF antagonist pharmaceutical preparations with gold nanorods, preservation of the mechanism of action of TNF antagonist along with preliminary evaluation of novel PAT technology in imaging optical contrast agents conjugated with anti-rheumatic drugs. Further *in vivo* studies on animals are warranted to test the specific binding between such conjugates and targeted antigen in joint tissues affected by inflammation.

## 1. Introduction

Tumor necrosis factor (TNF) has been identified as a protein produced by the immune system that plays a major role in the suppression of tumor cell proliferation [1]. TNF- $\alpha$  over-expression has been found in patients with acute and chronic inflammatory arthritis both in disease target tissues and in the systemic circulation [1–5]. Because TNF has been implicated as one of the critical pathologic cytokines when over-expressed in the inflammatory cascade, much work has been done

to inhibit or antagonize TNF. Three drugs inhibiting TNF, Etanercept (fusion protein), Adalimumab (D2E7) (human monoclonal antibody) and Infliximab, (chimeric monoclonal antibody) have been developed and are currently FDA approved for various types of inflammatory diseases. Although the role of pro-inflammatory cytokines such as TNF- $\alpha$  in the pathogenesis of inflammatory diseases has been shown to be significant, there is a large inter- and intra-individual variability in the level of cytokine expression [6, 7]. Obtaining accurate information on cytokine expression in joints affected by inflammatory arthritis could be helpful in optimizing and/or

<sup>4</sup> Author to whom any correspondence should be addressed.

evaluating the efficacy of biological drugs. Currently, there is no noninvasive nonionizing molecular imaging modality with both high sensitivity and good spatial resolution which can enable drug delivery monitoring and therapeutic evaluation of inflammatory joint diseases.

Photoacoustic tomography (PAT), also referred to as optoacoustic tomography or thermoacoustic tomography, is an emerging hybrid imaging modality that is noninvasive, nonionizing, with high sensitivity, satisfactory imaging depth and good temporal and spatial resolution [8–21]. In SPAT, a short-pulsed laser source is used to illuminate the tissue sample and generate photoacoustic waves due to thermoelastic expansion. Then the signals are measured by wide-band ultrasonic transducers to reconstruct the image of the sample. Therefore, the contrast of PAT is based on the optical absorption in biological tissues, but its resolution is not limited by optical diffusion or multiple photon scattering but instead by the bandwidth of detected photoacoustic waves [22]. Because ultrasonic waves are much less scattered in biological tissues than light, PAT depicts subsurface joint tissue structures much more accurately than optical imaging. In other words, PAT overcomes the resolution disadvantage of optical imaging and the contrast disadvantage of ultrasound imaging. Moreover, like conventional optical technologies, PAT also presents a unique ability in tracing optical contrast agents in biological tissues. Employing laser-based PAT, the dynamic distributions of gold nanoshells and indocyanine green (ICG) based contrast agents in small-animal brains have been imaged with both high spatial resolution and satisfactory sensitivity [23, 24].

One of the essential parts of this study is the use of gold nanorods to enhance the contrast in photoacoustic imaging. Gold nanoparticles are particularly useful in optical applications due to their exceptionally strong optical responses in the visible and NIR spectral range [25–34]. The combination of the unique optical and biological properties of gold nanoparticles makes them a good choice for optical contrast agent. Two important applications of gold nanoparticles in optical imaging include light scattering imaging and photoluminescence imaging, both presenting high sensitivity and having the ability to visualize single and multiple gold nanoparticles in biological cells. In comparison with these established modalities, PAT has the unique ability of imaging contrast agents in deeply embedded tissue with excellent spatial resolution, although the imaging sensitivity may not be as good. PAT is utilizing the strong optical absorption of gold nanoparticles which is due to localized surface-plasmon resonance (LSPR). This is a classical effect in which the electromagnetic field from the light source drives the collective oscillations of free electrons of metallic nanoparticles into resonance. The smaller peak in the 500 nm range is due to the plasmon oscillation perpendicular to the axis of the rod, while the strong NIR peak, which is tunable by varying the nanorod aspect ratio, originates from the longitudinal oscillations of plasmons along the main axis. Since NIR light transmits through tissue more efficiently than visible light, the additional plasmon resonance makes nanorods promising candidates for *in vivo* diagnostic and therapeutic applications. Gold nanorods are unique also because of their sharp resonance and their

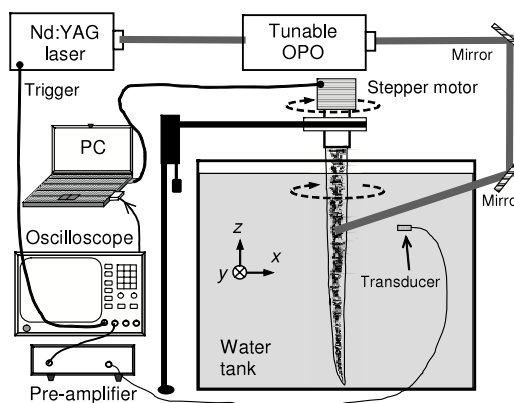


Figure 1. Schematic of the PAT system.

relatively small size, with their diameters approaching the molecular scale.

The long-term objective of this research is to realize molecular imaging and drug delivery monitoring for inflammatory joint diseases with both excellent sensitivity and high resolution by using novel PAT technology aided by the newly developed gold nanorod contrast agent. Gold nanoscale, and more specifically nanorod conjugates, also may have pharmaceutical benefits in light of the history of gold applications in various types of inflammatory arthritis. As an essential step toward our ultimate goal, in this study the bioconjugation between gold nanorods and Etanercept, an FDA-approved anti-rheumatic drug that inhibits TNF- $\alpha$ , was verified through ELISA experiment. The feasibility of PAT in imaging the distribution of the gold-nanorod-conjugated drug in regional articular tissues was also validated through the study on a rat tail joint model.

## 2. Methods

### 2.1. Imaging system

A PAT prototype system for joint imaging was employed in this study, as shown in figure 1. This system has been introduced before in [35]. The wavelength of the laser light was tuned by the OPO to 680 nm, which is close to the absorption peak of the employed gold nanorods and enabled good penetration depth in biological tissues. For 2D imaging of a joint cross section, a circular scan was conducted with the sample rotated axially while keeping the transducer and the laser beam static. In order to cover a  $2\pi$  angle of view, the circular scan was conducted at 240 positions with a constant interval of  $1.5^\circ$ . To reconstruct a photoacoustic image presenting the heterogeneous optical absorption in the sample, a modified back-projection algorithm was employed [17, 36, 37]. The back-projection was performed in the time domain, where the positions of the absorbing objects were determined by the time-of-flight and the acoustic velocities in the sample. To reconstruct an image, the measured signals, after a derivative, were back-projected into the image space and then integrated over all receiving angles. The transducer (XMS-310, Panametrics) employed in this study had a central frequency of

10 MHz and a full width at half-maximum (FWHM) amplitude bandwidth of  $\sim 100\%$ .

## 2.2. Gold nanorods and anti-TNF- $\alpha$ conjugation

One of the key techniques involved in this study is the preparation of bioconjugates of gold nanorods with Etanercept molecules, complex anti-TNF- $\alpha$  antibodies. Gold nanorods with an aspect ratio of 3 (45 nm by 15 nm) and an absorption peak at 660 nm were synthesized [38–40]. Both oxygenated- and deoxygenated-hemoglobin, the two major intrinsic absorbing substances in articular tissues, have comparatively low optical absorption in the spectra region between 650 and 720 nm [41]. By setting the absorption peak of gold nanorods in this region, we will have better imaging depth and enhanced signal-to-noise ratio in imaging the gold-nanorod-based contrast agent in the joint.

The synthesized gold nanorods have a bilayer of surfactant hexadecyltrimethylammonium bromide (CTAB) on their surface which acts as a stabilizer to prevent aggregation. The nanorods have a net positive charge on their surface because of the stabilizer. Excess CTAB in the solution is removed by centrifugation at 5900 rpm for 60 min. The gold nanorods form a pellet at the bottom of the tube which was redispersed in deionized water. The gold nanorods are finally dispersed in deionized water to achieve a molar concentration of 0.01 M of gold in the solution. A layer of polyacrylic acid (PAA) is adsorbed onto the surface of gold nanorods by adding 1.5 ml of  $10 \text{ mg ml}^{-1}$  PAA solution to 1 ml of the gold nanorod solution [40]. The mixture is stirred for 3 h followed by two cycles of centrifugation and redispersion to remove excess PAA in the solution. The layer of PAA provides the  $-\text{COOH}$  functional group required for the conjugation. The PAA-coated nanorods are dispersed in 1 ml of PBS 6.0 buffer solution followed by the addition of  $100 \mu\text{l}$  of 0.2 M EDC(*N*-ethyl-*N'*-(3-dimethylaminopropyl) carbodiimide) and  $100 \mu\text{l}$  of 0.2 M NHS (*N*-hydroxy-succinimide) [42–46]. After waiting for 20 min, the reaction mixture is added to 12.5 mg of Etanercept. The EDC/NHS mixture forms an active ester intermediate with the gold nanorods which undergoes an amidation reaction with the  $-\text{NH}_2$  group in the anti-TNF- $\alpha$  to yield the conjugate. The reaction mixture is stored in a refrigerator at  $4^\circ\text{C}$  overnight following centrifugation and redispersion in the buffer to remove the unconjugated drug.

## 2.3. Sensitivity of PAT in detecting gold nanorods

Before the experiments on animals, we validated the maximum sensitivity of the current PAT system in detecting gold nanorods through a study on a well-controlled phantom. The gold nanorods were diluted with PBS buffer to a concentration of  $10^8$  nanorods  $\text{ml}^{-1}$ , that is of the order of 1 pM. Then the nanorod solution was injected into glass tubing with a 1.7 mm inner diameter which was put into the PAT system working at 680 nm. The orientation of the glass tubing was orthogonal to the ultrasound detection beam and the distance between the tubing and the transducer surface was 5 cm. The recorded signal intensity as a function of time is shown in figure 2. The gold nanorod solution was injected from 400 s; before

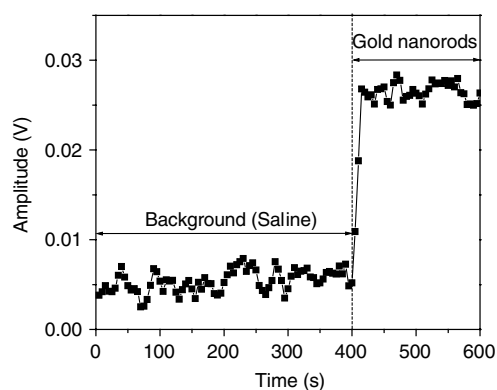


**Figure 2.** Photoacoustic signal from the gold nanorod solution with a concentration of 1 pM.

that time, the signal was from the background (i.e. saline). With concentration of the order of 1 pM, gold nanorods can be detected by the PAT system with a signal-to-noise ratio (SNR) up to 4.

## 2.4. ELISA experiment

An ELISA experiment was performed to prove the bioconjugation and to show that the anti-TNF- $\alpha$  drug conjugated with gold nanorods was still biologically active. Human TNF- $\alpha$  screening set purchased from ENDOGEN<sup>®</sup> was used. All experiments were performed in sterile conditions. The wells of the ELISA plate were coated with coating antibody and incubated overnight at room temperature. The coating antibody solution was aspirated next morning and  $300 \mu\text{l}$  of blocking buffer (4% BSA, 5% sucrose in D-PBS buffer) was added to all the wells and incubated for 1 h. The blocking buffer was then aspirated and the plate was allowed to dry for 1 h. Using reagent diluent (4% BSA in D-PBS buffer) lyophilized human TNF- $\alpha$  was reconstituted to a concentration of  $2000 \text{ pg ml}^{-1}$  and coated onto the wells. After incubation for 1 h the wells were washed with wash buffer three times. The conjugated nanorods were incubated for 1 h followed by three washes. Control experiments with unconjugated nanorods were also performed in parallel. To check for reproducibility/deviations in data, gold nanorods conjugated with Etanercept were placed in 18 wells, while the control (unconjugated gold nanorods) was placed in 10 wells. After three washes, absorbance of each well in the ELISA plate was measured using a microplate reader ( $\nu$  max kinetic microplate reader, Molecular Devices).

## 2.5. Rat model

Rheumatic disease rat models, including those with inflammatory arthritis, have been researched extensively and provide the opportunity to evaluate pathologic progression much more quickly than in humans [47–49]. Rat tail joints, due to their approximate size and morphological similarity to human finger and toe joints, provide reasonable examples for research purposes. In total, four adult Sprague Dawley rats ( $\sim 300$  g, Charles River Laboratory) were included in this study. Whole tails were harvested from the rat bodies within 1 min after the

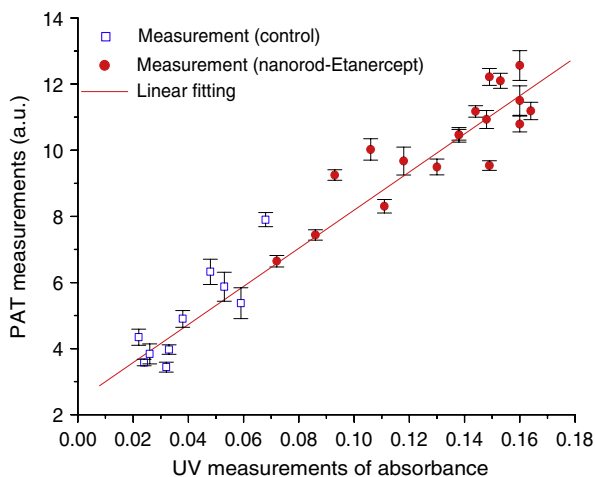


**Figure 3.** Photoacoustic measurements of the optical absorbance of ELISA wells in comparison with the UV/vis readouts.

(This figure is in colour only in the electronic version)

rats were sacrificed. An electrocautery device (SurgiStat, Valleylab) was then used to clot blood and seal vessels. The rat tail was placed in the PAT system along the Z axis (see figure 1). The first proximal segment of the rat tail was fixed on a rotational stage that, driven by a stepper motor, could rotate the tail around its axis. The imaged joint was about 2.5 cm from the rat trunk, where the diameter of the tail was  $\sim 8$  mm and the length of a segment was  $\sim 10$  mm. Administration of Etanercept-conjugated gold nanorods was conducted intra-articularly through a needle.

To obtain histological photographs, rat tails were saved in 10% buffered formalin for 3 d. Tails were then decalcified with formic acid for 4–7 d and monitored with a Faxitron MX-20 x-ray system. Once specimen decalcification was completed they were dehydrated with graded alcohol (Hypercenter XP by Shandon), embedded in paraffin (Paraplast Plus), cut into blocks and sectioned to  $7 \mu\text{m}$  thickness with a Reichert-Jung 20/30 metal knife (paraffin microtome). Hematoxylin and eosin staining of specimen sections on glass slides was conducted. Finally, the histological photographs of specimen sections were taken with a  $10\times$  magnification.

### 3. Results

#### 3.1. Outcomes of ELISA experiment

The absorbance of all the wells, including 18 wells where gold nanorods conjugated with Etanercept were incubated and 10 wells where unconjugated gold nanorods were incubated, are shown in table 1. The average absorbance of gold nanorod–Etanercept wells is  $0.132 \pm 0.028$ , while the average absorbance for control wells is  $0.040 \pm 0.016$ . The absorbance by the conjugated nanorods is more than three times higher compared to the control experiment. This result clearly indicates that the nanorods are conjugated with Etanercept and the nanorod–Etanercept conjugate is still active with a high affinity for TNF- $\alpha$ .

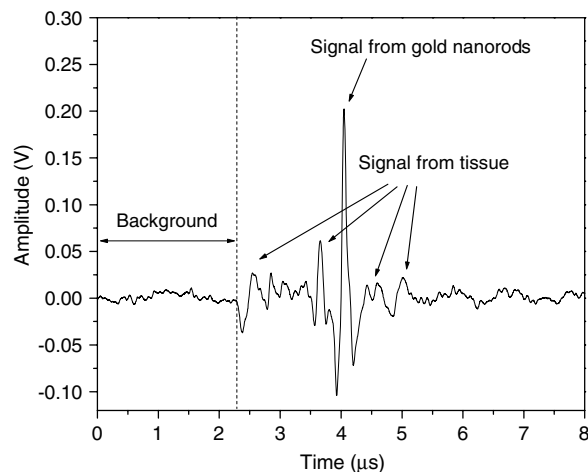


**Figure 4.** A-line photoacoustic signal from the imaged rat tail joint with the contrast enhanced by the gold nanorods.

**Table 1.** Absorbance of each well in the ELISA plate.

	Gold nanorod–Etanercept			Control	
	1	2	3	4	5
A	0.149	0.106	0.093	0.048	0.038
B	0.16	0.118	0.086	0.026	0.024
C	0.164	0.111	0.072	0.033	0.059
D	0.138	0.16	0.153	0.022	0.053
E	0.149	0.16	0.138	0.068	0.032
F	0.13	0.148	0.144		

After making the measurements with the microplate reader, the wells in the ELISA plate were also put in the PAT system working at 680 nm wavelength to examine the sensitivity and accuracy of PAT in quantifying the optical absorption from the conjugated gold nanorods. Considering the possible inhomogeneity of the gold nanorod distribution in each well, PAT measurement of each well was conducted four times each at different locations. The average photoacoustic signal intensity and the standard error for each well is shown in figure 3, where photoacoustic (PA) measurements present a good linear relationship with the readouts from UV/vis ( $p < 0.0001$ ). The small discrepancy between PAT results and UV/vis readouts may come from the fluctuation of laser energy and the inhomogeneous distribution of gold nanorods in each well. Besides the good correlation between PAT and UV/vis outcomes, we can also see clearly the difference between the PAT results from the gold nanorods–Etanercept conjugates and those from the control.

#### 3.2. Imaging on rat tail joints

2D photoacoustic cross-sectional imaging of rat joints *in situ* was conducted with laser light at 680 nm. Figure 4 shows an example A-line of the photoacoustic signal from the imaged rat tail joint. The signal from the gold nanorods diffused in intra-articular connective tissue can be recognized with an excellent SNR of up to 17, where the amplitude of the noise was measured from the background before the arrival of the signal

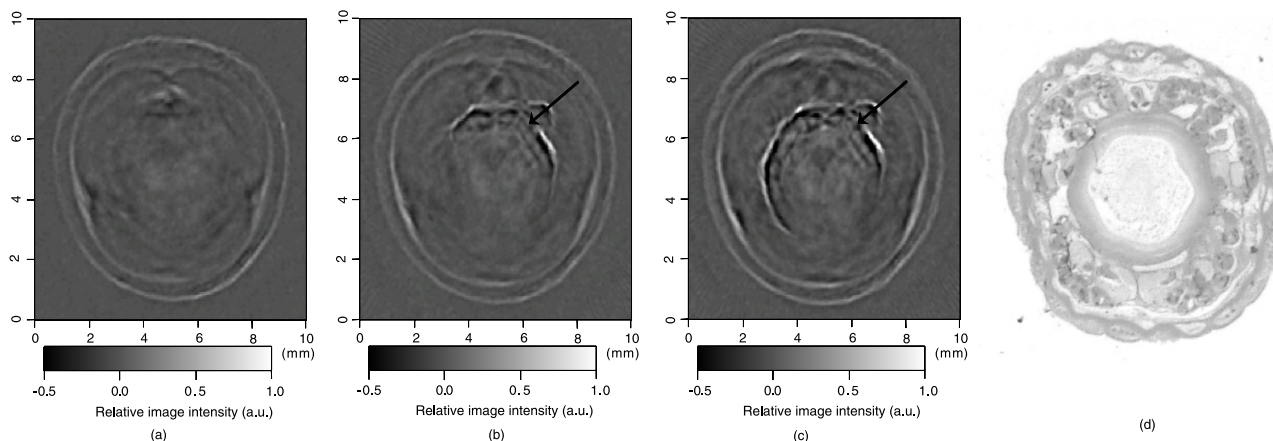


**Figure 5.** 2D cross-sectional PAT of a rat tail joint. (A) Image based on intrinsic contrast, which was taken before the administration of the contrast agent. Images taken after (B) the first and (C) the second administration of Etanercept-conjugated gold nanorods. For each administration, 0.025 ml agent with a 10 pM concentration was injected intra-articularly through the arrows in the images. (D) Histological photograph of a similar cross section in a rat tail joint showing the morphological features including intra-articular tissue, vessels and muscle.

from the tissue. The image in figure 5(A) was taken before the administration of Etanercept-conjugated gold nanorods, while the images in figures 5(B) and (C) were taken after the first and the second administrations of the contrast agent. The injections were conducted intra-articularly through a needle via the direction indicated by the arrows in the images. For both the first and the second injections, 0.025 ml agent with a gold nanorod concentration of  $10^9$  nanorods  $\text{ml}^{-1}$  (i.e. 10 pM) was introduced. The total number of gold nanorods introduced into the regional joint space for each injection was of the order of  $10^7$ . All the other experimental parameters for the images in figures 5(A)–(C) were the same, except that the specimen might be moved slightly during the administration of the contrast agent.

With the optical contrast enhanced by the gold nanorods, the contour of the intra-articular connective tissue is presented much more clearly in the images in figures 5(B) and (C) in comparison with the image in figure 5(A), which is based on the intrinsic tissue contrast. The hexagon shaped contour of the intra-articular connective tissue has been verified by the histological photograph of a similar cross section in a rat tail joint. The findings in figures 5(B) and (C) are also consistent: with more gold nanorods injected and diffused in the intra-articular connective tissue more areas of tissue were 'lightened'. This study has proved the capability of photoacoustic technology in tracing and quantifying gold-nanorod-based contrast agents in biological tissues. With our current PAT system, the spatially distributed gold nanorod contrast agent with a concentration down to 10 pM in biological tissues can be imaged with very good signal-to-noise ratio and high spatial resolution.

#### 4. Discussion

In conclusion, this study demonstrates the feasibility of a gold nanorod contrast agent to enhance joint imaging utilizing novel PAT technology. PAT, by combining the merits of both light and ultrasound, overcomes some limitations of

conventional optical and ultrasound imaging modalities. With our current system, PAT presents a maximum sensitivity of the order of 10 pM in imaging gold nanorods in conjugation with an anti-TNF- $\alpha$  drug. This sensitivity is parallel to conventional optical imaging in detection and quantifying a gold nanoparticle contrast agent [50–52]. Unlike conventional optical technologies, the spatial resolution of PAT is excellent (of the order of 250  $\mu\text{m}$ , and may be improved further by adjusting the detection bandwidth) in visualizing subsurface joint tissues and the spatially distributed contrast agent. The good resolution of PAT especially benefits the imaging of drug delivery and treatment effects in peripheral joints which are among the earliest to be affected by rheumatoid arthritis and are widely accepted to be the best markers of overall joint damage.

With further development of PAT technology, highly sensitive imaging of drug delivery in combination with high resolution high contrast anatomical imaging may be achieved through a single exam without the need for image fusion. PAT may enable investigators to follow the drug and/or the delivery vehicle on its journey through the body to ascertain whether successful drug uptake is occurring in the desired organ, such as arthritic joint tissues. Moreover, the good sensitivity of PAT to joint tissue morphological changes and functional hemodynamic changes may also make this technology promising in the evaluation of treatment efficacy. Other advantages of PAT which will also benefit laboratory research and future clinical practice involving molecular imaging include being nonionizing and relatively cheap when compared to other modalities such as magnetic resonance imaging and nuclear imaging.

In future studies, PAT of drug delivery monitoring will be conducted on arthritic animal models *in vivo* with systemic administration of drug-conjugated gold nanorods. Efficacy and toxicity of such applications will also be studied. Moreover, a multi-channel ultrasound unit with a well-designed ultrasonic array transducer will be employed to replace the single-element transducer for image acquisition. With this more advanced

imaging system, the sensitivity and resolution as well as the speed of PAT for molecular imaging may be improved significantly. We expect that PAT enhanced by a novel gold nanoparticle contrast agent may contribute considerably to the more efficient evaluation of drug effects in living laboratory animals and to optimize therapeutic decisions in human clinical practice in the future.

## Acknowledgment

This work was supported in part by the Arthritis National Research Foundation.

## References

- [1] Aggarwal B B, Shishodia S, Ashikawa K and Bharti A C 2002 The role of TNF and its family members in inflammation and cancer: lessons from gene deletion *Curr. Drug Targets Inflamm. Allergy* **1** 327–41
- [2] Steinerj G, Tohidast-Akrad M, Witzmann G, Vesely M, Studnicka-Benke A, Gal A, Kunaver M, Zenz P and Smolen J S 1999 Cytokine production by synovial T cells in rheumatoid arthritis *Rheumatology* **38** 202–13
- [3] Efthimiou P and Markenson J A 2005 Role of biological agents in immune-mediated inflammatory diseases *South. Med. J.* **98** 192–204
- [4] Fernandes J C, Martel-Pelletier J and Pelletier J P 2002 The role of cytokines in osteoarthritis pathophysiology *Biorheology* **39** 237–46
- [5] Cope A P, Aderka D, Doherty M, Englemann H, Gibbons D, Jones A C, Brennan F M, Maini R N, Wallach D and Feldmann M 1992 Increased levels of soluble tumor necrosis factor receptors in the sera and synovial fluid of patients with rheumatic diseases *Arthritis Rheum.* **35** 1160–9
- [6] Barrera P, Joosten L A, den Broeder A A, van de Putte L B, van Riel P L and van den Berg W B 2001 Effects of treatment with a fully human anti-tumour necrosis factor alpha monoclonal antibody on the local and systemic homeostasis of interleukin 1 and TNF $\alpha$  in patients with rheumatoid arthritis *Ann. Rheum. Dis.* **60** 660–9
- [7] Barrera P, Oyen W J G, Boerman O C and van Riel P L C M 2003 Scintigraphic detection of tumour necrosis factor in patients with rheumatoid arthritis *Ann. Rheum. Dis.* **62** 825–8
- [8] Oraevsky A A, Jacques S L, Esenaliev R O and Tittel F K 1994 Time-resolved optoacoustic imaging in layered biological tissues *Advances in Optical Imaging and Photon Migration* ed R R Alfano (New York: Academic) pp 161–5
- [9] Kruger R A 1994 Photo-acoustic ultrasound: pulse production and detection in 0.5% Liposyn *Med. Phys.* **21** 127–31
- [10] Kruger R A, Liu P-Y and Fang Y 1995 Thermoacoustic ultrasound (PAUS)-reconstruction tomography *Med. Phys.* **22** 1605–9
- [11] Oraevsky A A, Esenaliev R O, Jacques S L and Tittel S K 1996 Laser opto-acoustic tomography for medical diagnostics: principles *Proc. SPIE* **2976** 22–31
- [12] Hoelen C G A, de Mul F F M, Pongers R and Dekker A 1998 Three-dimensional photoacoustic imaging of blood vessels in tissue *Opt. Lett.* **23** 648–50
- [13] Fainchtein R, Stoyanov B J, Murphy J C, Wilson D A and Hanley D F 2000 Local determination of hemoglobin concentration and degree of oxygenation in tissue by pulsed photoacoustic spectroscopy *Proc. SPIE* **3916** 19–33
- [14] Oraevsky A A, Karabutov A A, Solomatina S V, Savateeva E V, Andreev V A, Gatalica Z, Singh H and Fleming R D 2001 Laser optoacoustic imaging of breast cancer *in vivo Proc. SPIE* **4256** 6–15
- [15] Kruger R A, Kiser W L Jr, Romilly A P and Schmidt P 2001 Thermoacoustic CT of the breast: pilot study observations *Proc. SPIE* **4256** 1–5
- [16] Esenaliev R O, Larina I V, Larin K V, Deyo D J, Motamedi M and Prough D S 2002 Optoacoustic technique for noninvasive monitoring of blood oxygenation: a feasibility study *Appl. Opt.* **41** 4722–31
- [17] Xu M and Wang L-H 2002 Time-domain reconstruction for thermoacoustic tomography in a spherical geometry *IEEE Trans. Med. Imaging* **21** 814–22
- [18] Kolkman R G M, Hondebrink E, Steenbergen W and de Mul F F M 2003 *In vivo* photoacoustic imaging of blood vessels using an extreme-narrow aperture sensor *IEEE J. Sel. Top. Quant.* **9** 343–6
- [19] Wang X, Pang Y, Ku G, Xie X, Stoica G and Wang L V 2003 Non-invasive laser-induced photoacoustic tomography for structural and functional imaging of the brain *in vivo Nat. Biotechnol.* **21** 803–6
- [20] Wang X, Pang Y, Ku G, Stoica G and Wang L V 2003 Three-dimensional laser-induced photoacoustic tomography of the mouse brain with the skin and skull intact *Opt. Lett.* **28** 1739–41
- [21] Zhang H F, Maslov K, Stoica G and Wang L-H 2006 Functional photoacoustic microscopy for high-resolution and noninvasive *in vivo* imaging *Nat. Biotechnol.* **24** 848–51
- [22] Xu M and Wang L-H 2002 Time-domain reconstruction for thermoacoustic tomography in a spherical geometry *IEEE Trans. Med. Imaging* **21** 814–22
- [23] Wang X, Ku G, Wegiel M A, Bornhop D J, Stoica G and Wang L V 2004 Noninvasive photoacoustic angiography of animal brains *in vivo* with near-infrared light and an optical contrast agent *Opt. Lett.* **29** 730–2
- [24] Wang Y, Xie X, Wang X, Ku G, Bill K L, O'Neal D P, Stoica G and Wang L V 2004 Photoacoustic tomography of a nanoshell contrast agent in the *in vivo* rat brain *Nano Lett.* **4** 1689–92
- [25] Cognet L, Tardin C, Boyer D, Choquet D, Tamarat P and Lounis B 2003 Single metallic nanoparticle imaging for protein detection in cells *Proc. Natl Acad. Sci. USA* **100** 11350–5
- [26] West J L and Halas N J 2003 Engineered nanomaterials for biophotonics applications: improving sensing, imaging, and therapeutics *Annu. Rev. Biomed. Eng.* **5** 285–92
- [27] Brongersma M L 2003 Nanoscale photonics: nanoshells: gifts in a gold wrapper *Nat. Mater.* **2** 296–7
- [28] Sokolov K, Follen M, Aaron J, Pavlova I, Malpica A, Lotan R and Richards-Kortum R 2003 Real-time vital optical imaging of precancer using anti-epidermal growth factor receptor antibodies conjugated to gold NPs *Cancer Res.* **63** 1999–2004
- [29] Hirsch L R, Jackson J B, Lee A, Halas N J and West J L 2003 A whole blood immunoassay using gold nanoshells *Anal. Chem.* **75** 2377–81
- [30] Oraevsky A A, Karabutov A A and Savateeva E V 2001 Enhancement of optoacoustic tissue contrast with absorbing NPs *European Conf. on Biomedical Optics; Proc. SPIE* **4434** 60–9
- [31] Copland J A, Eghtedari M, Popov V L, Kotov N, Mamedova N, Motamedi M and Oraevsky A A 2004 Bioconjugated gold NPs as a molecular based contrast agent: implications for imaging of deep tumors using optoacoustic tomography *Mol. Imaging Biol.* **6** 341–9
- [32] Wang H, Huff T B, Zweifel D A, He W, Low P S, Wei A and Cheng J-X 2005 *In vitro* and *in vivo* two-photon luminescence imaging of single gold nanorods *Proc. Natl Acad. Sci. USA* **44** 15752–6
- [33] Huang X, El-Sayed I H, Qian W and El-Sayed M A 2006 Cancer cell imaging and photothermal therapy in the near-infrared region by using gold nanorods *J. Am. Chem. Soc.* **128** 2115–20

- [34] Durr N J, Larson T, Smith D K, Korgel B A, Sokolov K and Ben-Yakar A 2007 Two-photon luminescence imaging of cancer cells using molecularly targeted gold nanorods *Nano Lett.* **7** 941–5
- [35] Wang X, Chamberland D L, Carson P L, Fowlkes J B, Bude R O and Jamadar D A 2006 Imaging of joints with laser-based photoacoustic tomography: an animal study *Med. Phys.* **33** 2691–7
- [36] Xu M and Wang L-H 2005 Universal back-projection algorithm for photoacoustic-computed tomography *Phys. Rev. E* **71** 016706
- [37] Wang X, Xu Y, Xu M, Yokoo S, Fry E S and Wang L-H 2002 Photoacoustic tomography of biological tissues with high cross-section resolution: reconstruction and experiment *Med. Phys.* **29** 2799–805
- [38] Nikoobakht B and El-Sayed M A 2003 Preparation and growth mechanism of gold nanorods (NRs) using seed-mediated growth method *Chem. Mater.* **15** 1957–62
- [39] Murphy C J and Jana N R 2002 Controlling the aspect ratio of inorganic nanorods and nanowires *Adv. Mater.* **14** 80–2
- [40] Jain P K, Lee K S, El-Sayed I H and El-Sayed M A 2006 Calculated absorption and scattering properties of gold nanoparticles of different size, shape, and composition: applications in biological imaging and biomedicine *J. Phys. Chem. B* **110** 7238–48
- [41] Weissleder R 2001 A clearer vision for *in vivo* imaging *Nat. Biotechnol.* **19** 316–7
- [42] Gole A and Murphy C J 2005 Biotin–streptavidin-induced aggregation of gold nanorods: tuning rod–rod orientation *Langmuir* **21** 10756–62
- [43] Lee J, Govorov A O, Dulka J and Kotov N A 2004 Bioconjugates of CdTe nanowires and Au nanoparticles: plasmon–exciton interactions, luminescence enhancement and collective effects *Nano Lett.* **4** 2323–30
- [44] Wang S, Mamedova N, Kotov N A, Chen W and Studer J 2002 Antigen/antibody immunocomplex from CdTe nanoparticle bioconjugates *Nano Lett.* **2** 817–22
- [45] Mamedova N N, Kotov N A, Rogach A L and Studer J 2001 Protein–CdTe nanoparticle conjugates: preparation, structure and interunit energy transfer *Nano Lett.* **1** 281–6
- [46] El-Sayed I, Huang X and El-Sayed M 2005 Surface plasmon resonance scattering and absorption of anti-egfr antibody conjugated gold nanoparticles in cancer diagnostics: applications in oral cancer *Nano Lett.* **5** 829–34
- [47] Hammer R E, Maika S D, Richardson J A, Tang J-P and Taurog J D 1990 Spontaneous inflammatory disease in transgenic rats expressing HLA-B27 and human  $\beta$ 2-m: an animal model of HLA-B27-associated human disorders *Cell* **63** 1099–112
- [48] Wooley P H 1991 Animal models of rheumatoid arthritis *Curr. Opin. Rheumatol.* **3** 407
- [49] Breban M, Hammer R E, Richardson J A and Taurog J D 1993 Transfer of the inflammatory disease of HLA-B27 transgenic rats by bone marrow engraftment *J. Exp. Med.* **178** 1670–16
- [50] Csáki A *et al* 2003 The optical detection of individual DNA-conjugated gold nanoparticle labels after metal enhancement *Nanotechnology* **14** 1262–8
- [51] Loo C *et al* 2004 Nanoshell-enabled photonics-based imaging and therapy of cancer *Tech. Can. Res. Treat.* **3** 33–40
- [52] Oldenburg A L, Hansen M N, Zweifel D A and Wei A 2006 Plasmon-resonant gold nanorods as low backscattering albedo contrast agents for optical coherence tomography *Opt. Express* **14** 6724–38